Acta Biomaterialia xxx (xxxx) xxx

Contents lists available at ScienceDirect

Acta Biomaterialia

journal homepage: www.elsevier.com/locate/actbio

Injectable hyaluronic acid and platelet lysate-derived granular hydrogels for biomedical applications

Bárbara B. Mendes[a,b], Andrew C. Daly[c], Rui L. Reis[a,b], Rui M.A. Domingues[a,b,*], Manuela E. Gomes[a,b,*], Jason A. Burdick[c,*]

[a] 3B's Research Group, I3Bs – Research Institute on Biomaterials, Biodegradables and Biomimetics, University of Minho, Headquarters of the European Institute of Excellence on Tissue Engineering and Regenerative Medicine, Avepark, Zona Industrial da Gandra, 4805-017 Barco – Guimarães, Portugal
[b] ICVS/3B's – PT Government Associate Laboratory, Braga/Guimarães 4805-017, Portugal
[c] Department of Bioengineering, University of Pennsylvania, USA

ARTICLE INFO

Article history:
Received 23 July 2020
Revised 25 October 2020
Accepted 27 October 2020
Available online xxx

Keywords:
Bioactive
platelet lysate
hyaluronic acid
microgels

ABSTRACT

Towards the repair of damaged tissues, numerous scaffolds have been fabricated to recreate the complex extracellular matrix (ECM) environment to support desired cell behaviors; however, it is often challenging to design scaffolds with the requisite cell-anchorage sites, mechanical stability, and tailorable physicochemical properties necessary for many applications. To address this and to improve on the properties of hyaluronic acid (HA) hydrogels, we combined photocrosslinkable norbornene-modified HA (NorHA) with human platelet lysate (PL). These PL-NorHA hybrid hydrogels supported the adhesion of cells when compared to NorHA hydrogels without PL, exhibited tailorable physicochemical properties based on the concentration of individual components, and released proteins over time. Using microfluidic techniques with on-chip mixing of NorHA and PL and subsequent photocrosslinking, spherical PL-NorHA microgels with a hierarchical fibrillar network were fabricated that exhibited the sustained delivery of PL proteins. Microgels could be jammed into granular hydrogels that exhibited shear-thinning and self-healing properties, enabling ejection from syringes and the fabrication of stable 3D constructs with 3D printing. Again, the inclusion of PL enhanced cellular interactions with the microgel structures. Overall, the combination of biomolecules and fibrin self-assembly arising from the enriched milieu of PL-derived proteins improved the bioactivity of HA-based hydrogels, enabling the formation of dynamic systems with modular design. The granular systems can be engineered to meet the complex demands of functional tissue repair using versatile processing techniques, such as with 3D printing.

1. Introduction

Tissues are hierarchically structured over different length scales and comprise multiple cell populations surrounded by a dynamic and bioactive extracellular matrix (ECM) [1]. ECM is a complex network of fibrous structural proteins (e.g., collagen, elastin), glycoproteins (e.g., laminin, fibronectin), glycosaminoglycans (GAGs) (e.g., heparan-sulfates, hyaluronic acid (HA)), and proteoglycans (e.g., aggrecan, versican) that may interact with growth factors and cytokines [2,3]. These ECM components are actively interconnected to establish unique compositions and topographies, which are crucial to provide structural and biochemical support to cells and to ultimately control cell behaviors, such as proliferation, growth, migration and differentiation [4]. Particularly, GAGs due to their high negative charge can establish strong electrostatic interactions with several soluble factors [5], which is further enhanced with van der Waals forces, hydrogen bonds, and hydrophobic interactions [6]. Thereby, ECM can dynamically and locally modulate the spatiotemporal presentation of soluble and immobilized molecules, and their subsequent signaling mechanisms [5]. In the context of tissue engineering and regenerative medicine (TERM) strategies, it is of utmost importance to develop effective engineered matrices that recapitulate such hierarchical fiber-based architectures and that introduce key cell instructive elements [7,8].

Hydrogels have been widely exploited as mimics of the ECM due to their hydrated network and unique physicochemical properties that can be tuned to precisely regulate cellular behaviors [9]. Additionally, hydrogels can be engineered to be injectable or *in situ* gelling, enhancing their clinical translation through the use of minimally invasive approaches while homogenously

* Corresponding authors.
E-mail addresses: ruimadomingues@i3bs.uminho.pt (R.M.A. Domingues), megomes@i3bs.uminho.pt (M.E. Gomes), burdick2@seas.upenn.edu (J.A. Burdick).

https://doi.org/10.1016/j.actbio.2020.10.040
1742-7061/

incorporating cells and bioactive elements within any defect size (or shape) [10,11]. Despite these advances, the majority of injectable hydrogels do not meet the complex demands of tissue repair since they do not recreate the organization, bioactivity, and mass transport properties of the native ECM [10,11].

Several research groups have recently proposed bottom-up engineering strategies to process hydrogels as hydrogel microparticles (HMPs, or microgels) [12,13]. The advantages of HMPs over traditional bulk hydrogels include: significant porosity (or void space), enhanced surface area, building blocks with modular design (e.g., composition, size, and contents), and a controlled mechanical response that depends on the polymer type and crosslinking degree [12,13]. Moreover, HMPs have gained interest in broader TERM through the creation of physicochemical gradients and tissue/disease models [13–16].

It was recently demonstrated that the agglomeration of HMPs in the jammed state produces granular hydrogels [12], enabling their combination with printing techniques to produce three-dimensional (3D) structures [16,17]. Cells can move within the porosity of the packed structure and spread, thereby maximizing cell–cell interactions and the synthesis of endogenous ECM, already at an early stage of the assembled constructs [18–20]. To take advantage of the potential benefits of granular systems to envision clinical applications, it is pivotal that the design of these advanced strategies recreate the physicochemical features of the native tissues [12,13]. These include cell anchorage sites and other bioactive cues, biodegradability, and xeno-free and clinically translatable processing.

HA is a non-sulfated GAG component in the native ECM that is expressed throughout the body at a concentration and molecular weight that varies by tissue source and body location [21,22]. Due to its crucial role in the ECM function, HA has been widely explored in the design of engineered biomaterials [23]. The limited bioactivity and adhesive properties of HA have been improved through the incorporation of RGD or bioactive proteins in order to maximize biomaterial-cell interactions and to develop efficacious cell-instructive biomaterials [23–26]. Our study engineers HA-based hydrogels with improved cell adhesion, high cell spreading, and tunable chemical and physical properties by incorporating platelet lysate (PL) that is recognized as an inexpensive source of biological molecules (e.g., growth factors, cytokines, self-assembling scaffolding proteins like fibrinogen) [27]. Specifically, PL was incorporated within a photocrosslinked norbornene-modified HA (NorHA) network with clotting factors to trigger fibrinogen polymerization (Fig. 1). We aimed to demonstrate that the system (1) possesses a similar fiber-based architecture to the native ECM due to the self-assembly of fibrinogen monomers; (2) contains an enriched milieu of key temporary ECM proteins with natural cell binding motifs; (3) preserves PL-derived protein bioactivity and fibrin polymerization; and (4) can be processed into relevant structures (e.g., microgels with microfluidics) and with precision technologies (e.g., 3D printing of granular hydrogels). In hydrogel and microgel formats, we evaluate the presence of an ECM-mimetic hierarchical fibrin matrix, characterize mechanical and rheological properties, analyze the degradation behavior and subsequent release of therapeutically-relevant biomolecules, and assess the adhesion and spreading of mesenchymal stromal cells (MSCs).

2. Materials and Methods

2.1. Hydrogel and microgel synthesis and fabrication

Synthesis of norbornene-modified hyaluronic acid (NorHA): Prior to NorHA synthesis, sodium hyaluronate was converted to its tetrabutylammonium salt (HA-TBA), as previously described [28]. Briefly, sodium hyaluronate (75 kDa, Lifecore Biomedical) was dissolved in deionized (DI) water at 2 wt.% and 3 g of Dowex 50W hydrogen form exchange resin (Sigma-Aldrich) was added to 1 g of sodium hyaluronate for 2 h at room temperature (RT). The resin was filtered off by vacuum filtration (2, Whatman® qualitative filter paper, Sigma-Aldrich) and the filtrate was titrated with diluted TBA hydroxide solution (TBA-OH, Thermo Fisher Scientific) to a pH of ≈7.03-7.05, and then flash-frozen in liquid nitrogen and lyophilized (0.050 mBar and -52ºC, Labconco). Proton nuclear magnetic resonance spectroscopy (^{1}H NMR, DMX 360 MHz, Bruker) was used to characterize the final product.

NorHA was synthesized by coupling HA-TBA with 5-norbornene-2-methylamine (3 molar ratio to HA-TBA repeat units, Tokyo Chemical Industry) in the presence of ditert-butyl dicarbonate (Boc2O, 0.4 molar ratio to HA-TBA repeat units, Sigma-Aldrich) and 4-(dimethylamino)pyridine (DMAP, 1.5 molar ratio to HA-TBA repeat units, Sigma-Aldrich), and dissolved in anhydrous dimethyl sulfoxide (DMSO, Sigma-Aldrich). The mixture was stirred for 20 h at 45 ºC under a nitrogen atmosphere. Then, cold water (5x) was added to quench the reaction and the solution was dialyzed (Regenerated Cellulose Dialysis Membrane Tubing 6 to 8 kDa, Spectrum®) against 1 L of DI water with 0.25 g of sodium chloride (NaCl) for 4 days. After dialysis, 0.75 g of NaCl was added to 100 mL of dialyzed solution and it was precipitated into 10-fold excess cold acetone. The pellet was resuspended in cold DI water, dialyzed (Regenerated Cellulose Dialysis Membrane Tubing 12 to 14 kDa, Spectrum®) for 3 days, flash-frozen in liquid nitrogen and lyophilized (0.050 mBar and -52ºC, Labconco). ^{1}H NMR was used to determine the functionalization of HA by norbornene (≈ 30% of HA repeat units were modified with norbornene groups, Fig. S1).

PL preparation: Human PL (PLTMax®, Mill Creek Life Sciences) was defrosted at room temperature (RT), aliquoted and stored at -80 ºC. Prior to use, PL solution was defrosted at RT and briefly spun down to remove any platelet fragments. The mean fibrinogen level was 350 ± 124 μg mL^{-1} (experiment was conducted by Mill Creek Life Sciences), which is similar to the previously reported fibrinogen concentration in PL prepared from freeze-thaw cycles of pooled human expired platelets batches [29].

Hydrogel formation: Hydrogels across various compositions were prepared from separate precursor solutions at 1:1 volume ratio. For precursor solution 1, NorHA was dissolved in PBS (2 or 4 w/v) in the presence of dithiothreitol (DTT, Sigma-Aldrich) at 0.8 mol of thiols to 1 mol of norbornenes and 0.1 w/v lithium phenyl(2,4,6-trimethylbenzoyl)phosphinate (LAP, Tocris Bioscience). Precursor solution 2 consisted of either phosphate-buffered saline (PBS, Sigma-Aldrich) or human PL solution.

Specific compositions are as follows:

1. NorHA hydrogel via mixing of precursor solution 1 and PBS (precursor solution 2).
2. NorHA hydrogel with cell-adhesive RGD oligopeptide (GenScript) via the addition of 4 mM of thiolated RGD motifs to precursor solution 1 (NorHA) and PBS (precursor solution 2), as previously described [30].
3. NorHA hydrogel with PL proteins in solution via mixing of precursor solution 1 and PL (precursor solution 2), without induction of the coagulation cascade.
4. PL-NorHA hydrogels embedded with fibrillar structures, clotting factors via the addition of thrombin from human plasma (4 U mL^{-1}, Sigma-Aldrich) and calcium chloride (10 mM, MERCK) to solution 1 and mixing with PL (precursor solution 2), to induce PL coagulation cascade.

Both precursor solutions (1 and 2) were mixed and hand extruded onto glass coverslips to form hydrogel films. The mixture was incubated for 20 minutes at RT to allow PL matrix polymerization, and then the hydrogels were cured by visible light exposure

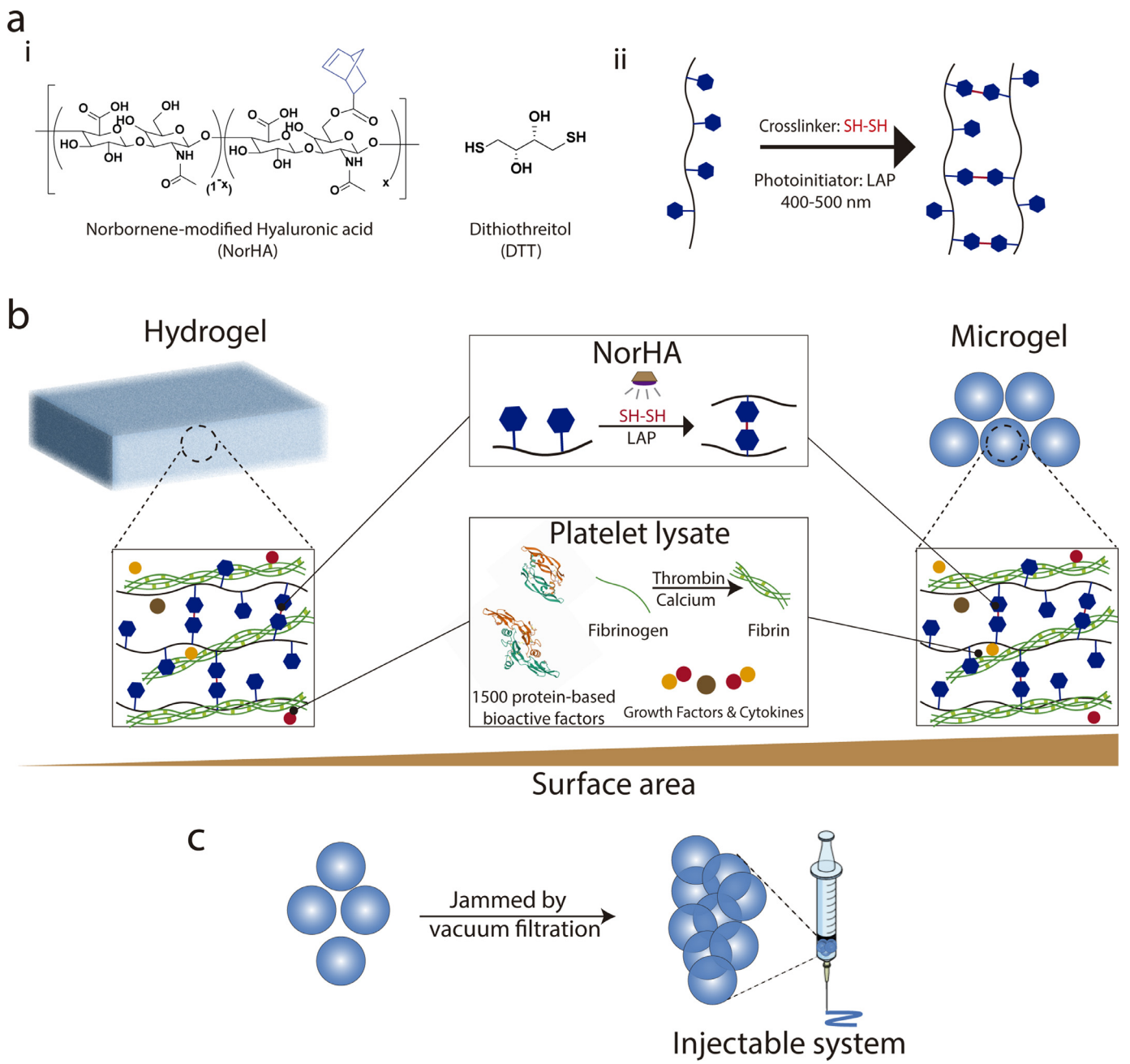

Fig. 1. Fabrication of platelet lysate-based hyaluronic acid hydrogels and microgels. a) (i) Chemical structures of components incorporated into norbornene-modified hyaluronic acid (NorHA) hydrogels and (ii) schematic representation of thiol-ene reaction, in which NorHA (≈30% modification) undergoes photocrosslinking through a thiol-ene reaction in the presence of a di-thiol (DTT) crosslinker, a visible light photoinitiator (LAP), and exposure to visible light. b) Schematic representation of networks formed via the homogenous mixing of NorHA and human platelet lysate. Thiol-ene reaction employed to crosslink the NorHA hydrogel. Fibrinogen polymerization within the PL is initiated by adding thrombin and calcium ions. c) Microgels can be jammed through vacuum filtration into a solid that can be extruded from a syringe or processed with 3D printing.

(Exfo Omnicure S1500 lamp, 400-500 nm filter, 26 mW cm^{-2}) for 5 minutes. The final hydrogels were composed of 50 vol.% of PL (or PBS) and 1 or 2 w/v NorHA concentrations, and the hydrogel experimental groups were named NorHA, NorHA RGD, NorHA proteins and PL-NorHA.

Microfluidic device fabrication and microgel formation: The mold of the microfluidic device was fabricated by micro-resolution stereolithography (MicroFine Green Resin, Proto Labs) and the desired microfluidic device was further produced by polydimethylsiloxane (PDMS, Sylgard™ 184, Ellsworth adhesives, USA) replica molding process as previously optimized [17]. Device features include four inlets (precursor solution 1 and 2, and two-side inlets for oil flow) and one outlet for droplets, a T-junction for the creation of polymer aqueous droplets into the oil flow, and a serpentine path to allow the mixing of the precursor solutions.

Mineral oil (light Fisher Chemical, Thermo Fisher Scientific) supplemented with 2 vol.% span 80 (Sigma-Aldrich) at flow rate of 5 μL min^{-1} (syringe pump, World Precision Instruments) was first introduced in the microfluidic device. Then, precursor solution 1 (NorHA or NorHA with clotting factors) and 2 (PBS or PL) were introduced at 1 μL min^{-1} and 2 μL min^{-1} flow rates, respectively. The precursor solutions were the same as described above for hydrogel formation. While flowing through the tubing at outlets (≈ 28 cm), the coagulation cascade was initiated and then the formed poly-

mer droplets were cured by visible light exposure (Exfo Omnicure S1500 lamp, 400–500 nm filter, 290 mW cm^{-2}). Microgels collected with mineral oil were centrifuged (1000 G for 5 min), purified by sequential washing steps with PBS and stored at 4 ºC until further use. The microgel experimental groups were NorHA and PL-NorHA.

2.2. Jammed granular hydrogels

Jammed microgel morphology: Thiolated fluorophores (GCKK-RHO) were prepared through standard solid phase peptide synthesis (PS3 automated peptide synthesizer, Protein Technologies) [31]. The fluorescent peptide (final concentration of 2 mM) was incubated in microgel suspensions for 30 min, coupled via thiol-norbornene photochemistry (0.05 w/v Irgacure 2959, Sigma-Aldrich) with UV light curing (Omnicure S1500, 320–390 nm filter, ≈5 min) and washed three times with PBS. Microgels were jammed by vacuum-driven filtration (Steriflip, 0.22 μm pores, Millipore) and then imaged with confocal microscopy. To quantify the empty area between the microgels, fluorescence images (~100 µm total depth, 5 µm per slice) were converted to 8-bit images. Then, an auto local threshold of 50 was applied in ImageJ.

Jammed microgel inks and printed structure stability: A modified stepper motor-based extruder with a 3D printer Revolution XL printer (Quintessential Universal Building Device, Inc.) was used for 3D printing [32]. Printing paths were processed into G-code by Slic3r and printed using Repetier hardware. Jammed microgel inks were loaded into a syringe (Microliter, Hamilton) and extruded through a 25 G needle at 40 mm min^{-1} printing speed. Single line filaments, lattice and cuboid structures (dimensions: 4.5 x 4.5 x 1 mm; width, length and height) were printed on a glass surface. Then, 3D printed structures were immersed in PBS and the maintenance of their printed shape was evaluated for 7 days. Single line filaments, lattice and cuboid structures were observed by fluorescence microscopy.

2.3. Hydrogel and microgel characterization

Microgel morphology: Fluorescein isothiocyanate (FITC)-Dextran (1 mg mL^{-1}, ≈2 MDa, Sigma-Aldrich) was added to the precursor solution 1 and fluorescence microscopy (Olympus BX51) was used to analyze microgel morphology after the PBS washing steps. Microgel diameter and roundness were further quantified by ImageJ software (National Institutes of Health).

Fibrin network analysis: For visualization of the fibrin networks within hydrogels, 9 μg of Alexa Fluor® 488 conjugated fibrinogen from human plasma (Thermo Fisher Scientific) was added to 1 mL of PL solution (precursor solution 2), and then images were acquired with confocal microscopy (SP5, Leica Microsystems). The fibrin networks within microgels were visualized by reflectance confocal microscopy (SP5, Leica Microsystems), using scattered light instead of fluorescence.

Rheological characterization: Rheological measurements were performed using an AR2000 stress-controlled rheometer (TA Instruments) fitted with a 20 mm diameter acrylic cone (59 min 42 s angle) and plate geometry using 27 µm (for hydrogel tests) or 1 mm (for microgel tests) gaps. For hydrogel rheological analysis, hydrogels were formulated as described above and precursor solutions were mixed immediately prior to testing. Time sweep tests were applied to study the polymerization kinetics of different formulations (0.5% strain, 1.0 Hz). After 20 min, hydrogels were cured by visible light (Exfo Omnicure S1500 lamp, 400−500 nm filter, 26 mW cm^{-2}) for 5 min. Frequency sweep tests (1% strain, 0.01 Hz to 100 Hz) were conducted after the hydrogel modulus plateaued and only the storage modulus (G′) values from 0.1 to 10 Hz frequencies are graphically represented. For microgel rheological properties, microgels were first jammed by vacuum-driven filtration and then placed on the rheometer for time sweep (0.5% strain, 1 Hz) and strain sweep (0.5% to 500% strain, 1 Hz) tests. To demonstrate self-recovery properties, the storage modulus (G′) values were evaluated under cycling strains (0.5% or 500% for 2 min each strain, 1 Hz).

Degradation behavior: Hydrogels were produced as described above (60 µL) and incubated in 300 µL of PBS, either alone or with 0.005 mg mL^{-1} (i.e., 3.75 – 15 U mL^{-1}, ~ 9.4 U mL^{-1}) hyaluronidase from bovine testes (Type IV-S, 750-3000 U mg^{-1} solid, Sigma-Aldrich). This value of enzyme concentration falls in between the physiological levels of hyaluronidase (0.0059 ± 0.0012 U mL^{-1} - human plasma to 38.5 U mL^{-1} - human ovaries) [33,34]. Jammed microgels (60 µL) were fabricated as described above and incubated in 300 µL of PBS or 0.005 mg mL^{-1} (i.e. 3.75 – 15 U mL^{-1}, ~ 9.4 U mL^{-1}) hyaluronidase at 37 ºC. At desired times, samples were centrifuged (1200 G for 15 min), releasate buffer was collected and replaced with fresh solution, and the releasate was stored at −20 °C. The timepoints were named as follows: D0 (30 minutes), D1 (1 day), D3 (3 days), D5 (5 days) and D7 (7 days). After one week, samples were fully degraded in hyaluronidase at 1 mg mL^{-1} (750-3000 U mg^{-1}, ~ 1875 U mL^{-1}), as previously performed [35] HA release was determined using a uronic acid assay [36], and PL-derived proteins were quantified via Pierce Bicinchoninic Acid Assay Kit (Thermo Fisher Scientific) according to the manufacturer's instructions. Degradation and protein release are represented as the cumulative release over time, according to the following Eq. (1).

$$\text{Cumulative release } (\%) = \left(\frac{M_x}{M_t}\ x\ 100\right) + \left(\frac{M_{x-1}}{M_t}\ x\ 100\right) \qquad (1)$$

Where M_x is the amount of uronic acid/total protein content quantified at each timepoint, M_t is the amount of uronic acid/ total protein content in the entire hydrogel/microgel (sum of the amount of all the timepoints (D0, D1, D3, D5 and D7) and the amount quantified upon full hydrogel/microgel degradation), and M_{x-1} corresponds to the amount of uronic acid or total protein content of the previous timepoint(s).

2.4. In vitro *cell behavior*

Cell culture and immunofluorescence staining: Human mesenchymal stromal cells (MSCs, passage 3, Lonza) were cultured in α-MEM (Gibco) supplemented with 10% fetal bovine serum (FBS, Gibco) and 1% penicillin/streptomycin solution (Invitrogen) at 37 °C and 5% CO_2. Cells were trypsinized with 0.05% Trypsin (Gibco) and then resuspended in culture media without FBS. Hydrogels were produced as described above and incubated for 30 min in 150 µL medium before $3x10^3$ cells cm^{-2} MSCs (final volume of 300 µL per condition) were seeded and cultured for either 4 or 24 hours.

For staining procedures, samples were washed with PBS, fixed in 10% formalin (Thermo Fisher Scientific) for 15 min, washed with PBS and then permeabilized using 0.2 vol.% Triton X-100 in PBS for 10 min (Sigma-Aldrich). After washing, the samples were incubated with 1:200 v/v rhodamine conjugated phalloidin (Sigma-Aldrich) and 1:2000 v/v Hoechst 33342 (Life Technologies) for 20 min. Samples were washed in PBS and imaged with fluorescence microscopy. For measurements of cell spread area and cell aspect ratio, fluorescence images were converted to binary images to identify individual cells and a mean threshold was applied in ImageJ.

For microgel cell studies, rhodamine-thiol-tethered microgels were homogeneous mixed with MSCs at $1x10^6$ cells mL^{-1}, centrifuged at 1000 G for 5 min, jammed by vacuum-driven filtration and cultured for 1 or 7 days. Cells were labelled with Cell Tracker™ fluorescent probes (Green-CMFDA, 5µM) for 30 minutes prior to mixing for visualization. After culture, samples were

washed in PBS and then imaged using confocal microscopy. Images represent z-stacks (~300 µm total depth, 5 µm per slice) and 3D analysis was performed with LASX software (Leica). For measurements of cell stained area, fluorescence images (~100 µm total depth, 5 µm per slice) were converted to 8-bit images, the images were thresholded to separate the signal from the background, and the area fraction (%) was determined in ImageJ.

2.5. Statistical analysis

Statistical analysis: All statistical analyses were performed using Graphpad Prism 7 software. Data are presented as mean ± standard deviation. All experiments were repeated as described in the text. Statistical comparisons were conducted using one-way analysis of variance (ANOVA) with Tukey's post hoc multiple comparison test, with $p<0.05$ denoting significance.

3. Results and Discussion

3.1. Development of hyaluronic acid hydrogels containing embedded platelet lysate fibrillar proteins

3.1.1. Hydrogel synthesis and characterization

In this study, HA was crosslinked into hydrogels through thiol-norbornene click chemistry, including HA modified with norbornenes (NorHA) at 30% of modification of disaccharide repeat units, dithiothreitol (DTT) crosslinker and visible light for hydrogel formation (Fig. 1a and Fig. S1), as optimized in previous studies [28,37,38]. Recently, we also demonstrated that NorHA with ≈30% of its repeat units functionalized with pendent norbornenes produces stable microgels; thus, we performed our experiments with this degree of modification of HA with norbornene groups [35]. The formulation could also be combined with clotting agents and PL and incubated for 20 minutes prior to light exposure to trigger a coagulation cascade.

For the analysis of the fibrillar structure, fluorescent fibrinogen was added to the PL solution and visualized by confocal microscopy (Fig. 2a-i,ii). Hydrogels at NorHA concentrations of 1 and 2 wt.% exhibited an interconnected and homogenous fibrillar architecture that resembles a typical hierarchical fibrin matrix. The induction of the coagulation cascade mimics the physiological process that occurs after injury - initiated by thrombin cleavage, which exposes the central domain of fibrinogen binding sites to induce the self-assembly of fibrin monomers and the formation of half-staggered two-stranded protofibrils [39]. When protofibrils achieve a threshold length, they start to associate laterally to form fibers that branch into a 3D network. The introduction of these multiscale properties recreates the complexity of the hierarchical organization of the native ECM from the nanoscale (e.g., fibrin fibrils) to the microscale (e.g., fibrin fibers), which is difficult to recreate using synthetic biomaterials.

To better understand the gelling kinetics and network properties of the produced hydrogel, their gelation process and viscoelastic properties were analyzed (Fig. 2b-i-iv). Before visible light irradiation (at 20 minutes), NorHA, NorHA proteins (i.e., without clotting agents) and PL-NorHA (i.e., addition of clotting agents) conditions exhibited a low storage modulus, with similar mechanics (G' ≈ 1-2 Pa and G'' ≈ 0.4-1 Pa). These results are in agreement with previous studies on scaffolds solely based on PL exhibit where limited stability and low mechanical properties were observed [27]. However, the elastic and viscous moduli increased when exposed to visible light due to the covalent photocrosslinking process via thiol-ene reaction and reached a storage moduli plateau within seconds (Fig. 2b-i-iv).

The PL-NorHA hydrogels (G': 593 ± 156 Pa – 1 wt.% and G': 3536 ± 159 Pa – 2 wt.%) exhibited a lower storage modulus than hydrogels with only NorHA (G': 1655 ± 238 Pa – 1 wt.% and G': 4845 ± 376 Pa – 2 wt.%) or NorHA with proteins (G': 1561 ± 75 Pa – 1 wt.% and G': 5324 ± 722 Pa – 2 wt.%). The reduction in moduli with the addition of PL and coagulation are potentially explained by the self-assembly of fibrinogen derived from the PL solution, which produces an interconnected network before HA photocrosslinking. This may create some steric hindrance to reduce HA macromer mobility or phase separation that limits the continuity of the HA hydrogel, impairing thiol-ene crosslinking after light exposure. Since both networks are entangled with each other, we can leverage this mechanism to modulate hydrogel mechanical properties.

3.1.2. Release of proteins from PL-containing hydrogels

HA biosynthesis and tissue turnover is regulated by three synthases and several hyaluronidases that can naturally catabolize HA with times ranging from hours to days [24,40] depending on the local enzyme concentration [41]. In our study, the *in vitro* degradation profiles of the hydrogels were evaluated either in buffer alone or in the presence of hyaluronidase at 0.005 mg mL^{-1}, with quantification of either uronic acid or total proteins over time (Fig. 2c). After 7 days, hyaluronidase was added to the remaining hydrogel for complete degradation. As expected, the overall time and rate of hydrogel degradation was faster in the presence of hyaluronidase (Fig. 2c-i,iii). There was also a correlation between the degradation time and crosslinking density, with the higher concentration of 2 wt.% degrading more slowly than the lower concentration of 1 wt.% (Fig. 2c-i,iii). Additionally, the PL-NorHA hydrogels degraded faster than NorHA (Fig. 2b-i,iii). As previously reported, when the network becomes loosely crosslinked, the degradation rate increases due to the rapid solubilization of HA and facilitated matrix diffusion of the enzyme [42]. Therefore, these findings are in agreement with our previous observations that the fibrin matrix formation decreases thiol-ene crosslinking density.

Unsurprisingly, the previously discussed hydrogel physical properties have a measurable impact on the temporal and spatial release of therapeutically-relevant PL proteins (Fig. 2c-ii,iv). In PL-based hydrogels, there is an obvious burst release of proteins at early times, followed by a general plateau until hydrogels reached complete degradation (or the end of the assay is reached). This release profile can be related to the release of the easily accessible proteins close to hydrogels surface, as well as of the abundant non-fibrillar and un-bound proteins (e.g., albumin) that compose these formulations. After this initial release, the degradation of the hydrogel released the remaining proteins (1 wt.% in the presence of hyaluronidase). In PL-NorHA 1 wt.% (in PBS alone) and 2 wt.% hydrogels (in PBS alone or with hyaluronidase), the proteins were retained in the hydrogel. In addition to the covalent photocrosslinking of the network (NorHA), PL-NorHA hydrogels contain a crosslinked fibrillar fibrin matrix. Therefore, the hydrogel degradation is not only due to the uronic acid release (HA degradation) but also to the fibrin matrix degradation, which shows high affinity to several proteins from PL (e.g., growth factors) [43,44]. Inherently, formulations with a low crosslink density exhibited a higher initial release of PL-derived proteins (92 ± 1 %) than formulations with 2 wt.% NorHA concentration (72 ± 2 %) in the presence of hyaluronidase. These findings indicate that the HA macromer concentration as well as fibrin matrix are parameters that can be explored to modulate the release of the hydrogel therapeutic cargo in a controlled and spatiotemporal manner.

3.1.3. In vitro *cell response to hydrogels*

MSCs were seeded on NorHA, NorHA-RGD and PL-NorHA hydrogels under serum-free conditions and their morphology was assessed after 4 hours and 1 day of *in vitro* culture (Fig. 3). As a

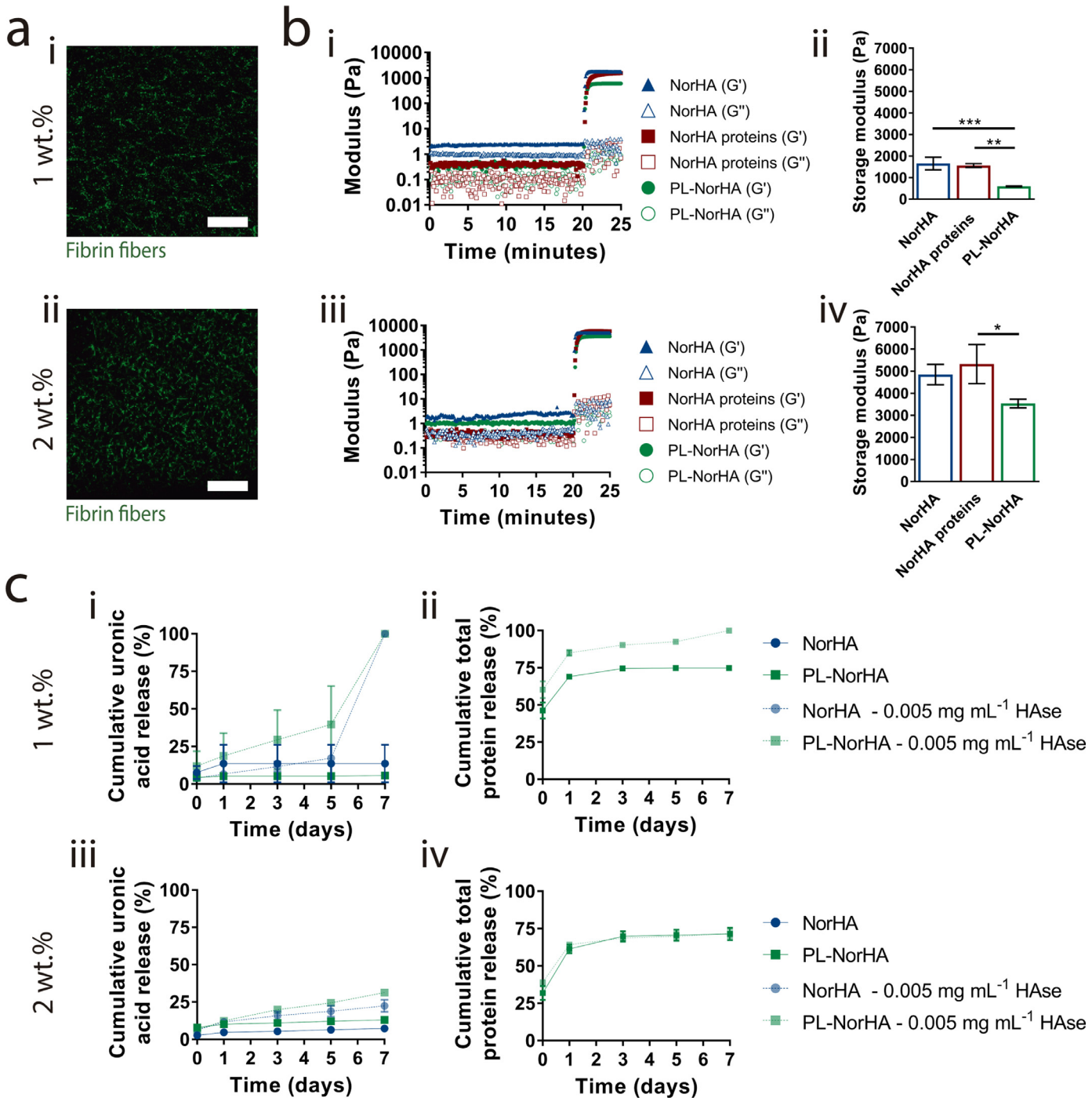

Fig. 2. Characterization of the mechanical and degradation behaviors of hydrogels. a) Fibrin (green) polymerized within (i) 1 wt.% and (ii) 2 wt.% PL-NorHA (NorHA plus coagulation cascade induction of fibrinogen from PL) hydrogels (scale bar 50 μm). b) Representative time sweeps (1.0 Hz, 0.5% strain, light introduced at 20 minutes) of the polymerization of NorHA, NorHA proteins (NorHA plus PL-derived proteins) and PL-NorHA hydrogels and average plateau storage moduli (G') at concentrations of (i, ii) 1 wt.% and (iii, iv) 2 wt.% from time-sweep tests (1.0 Hz, 0.5% strain), n= 3 independent experiments, mean ± SD * $p < 0.05$, ** $p < 0.01$, *** $p < 0.001$, one-way ANOVA with Tukey's multiple comparisons test. c) Cumulative uronic acid and total protein release during the degradation of (i, ii) 1 wt.% and (iii, iv) 2 wt.% hydrogels when incubated in PBS alone or with hyaluronidase at 0.005 mg mL $^{-1}$, n=3 independent experiments, mean ± SD (note: error bars in many groups are smaller than the symbols).

result of the enriched environment of protein-based bioactive factors, we explored the release of PL as substitute to bovine serum during culture. Similar to fetal bovine serum (FBS), PL provides important nutritional and macromolecular factors that exhibit important growth-promoting and transport properties [45]. These include albumin (represents ≈40 % of total PL proteins) that supports cell growth [46,47] and growth factors (e.g., platelet-derived growth factor, transforming growth factor-β, basic fibroblast growth factor) [48] that are responsible for numerous cell responses such as proliferation [49], chemotaxis [50] and angiogenesis promotion [51]. Moreover, although not studied here, the potential role of PL on promoting e.g. osteogenic or chondrogenic differentiation of stem/progenitor cells have also been suggested [52,53]. Studying MSCs biological response on PL-NorHA hydrogel system targeting a specific regenerative application would be therefore an interesting topic for further research.

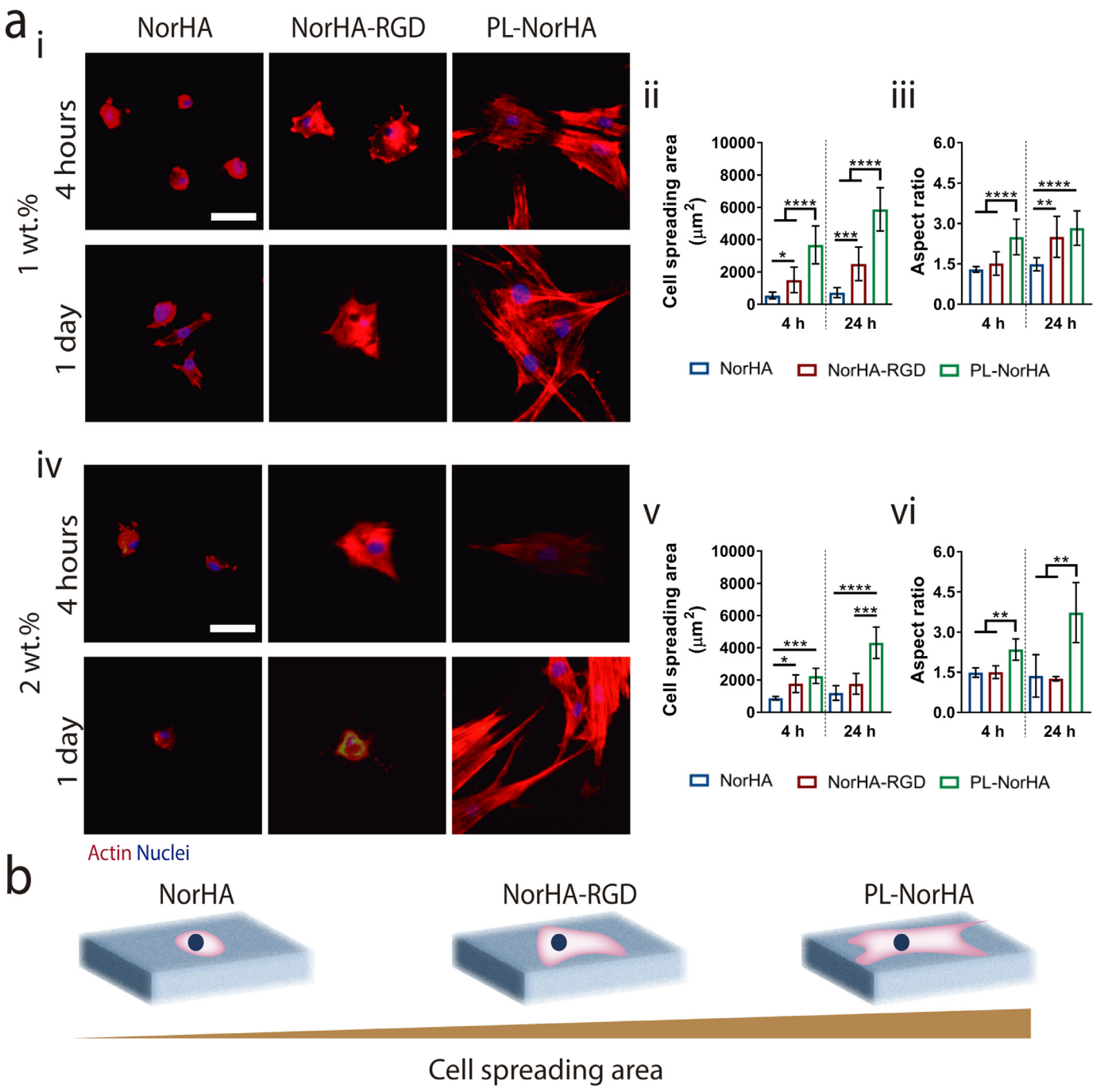

Fig. 3. *In vitro* evaluation of human MSC interactions with hydrogels. a) Representative fluorescence images (actin: red, nuclei: blue) and quantification of cell spreading and aspect ratio for MSCs cultured for either 4 hours or one day in serum-free medium on (i-iii) 1 wt.% or (iv-vi) 2 wt.% NorHA, NorHA-RGD (NorHA containing 2 mM RGD motifs) or PL-NorHA (NorHA plus coagulation cascade induction of fibrinogen from PL hydrogels). Scale bar 50 μm. (cell spreading area and aspect ratio: n ≥ 20 cells), mean ± SD, * $p < 0.05$, ** $p < 0.01$, *** $p < 0.001$, **** $p < 0.0001$ one-way ANOVA with Tukey's multiple comparisons test. b) Schematic representation of cell adhesion on hydrogel surfaces with various hydrogel formulations.

By the straightforward incorporation of PL proteins within NorHA hydrogels without any further chemical modifications, we avoid the use of chemical crosslinking methods (e.g., 1-ethyl-3-(3-dimethylaminopropyl)-carbodiimide (EDC) crosslinkers) and processing techniques (e.g., glutaraldehyde treatment) that produce potential toxic products and require extensive washing steps, which jeopardizes cytocompatibility and protein bioactivity [23,24,54,55].

Cells seeded on NorHA hydrogels exhibited generally rounded morphologies with some protrusions at 1 wt.% and 2 wt.% concentrations, displaying comparable cell spreading areas and aspect ratios over time (Fig. 3a). As expected, the incorporation of RGD integrin-binding motifs into NorHA hydrogels (1 wt.% and 2 wt.% NorHA-RGD) greatly enhanced cell spreading areas, although modest changes in aspect ratios were observed. Changes in MSC behavior were further observed in PL-NorHA formulations (1 wt.% and 2 wt.%), where cells adhered, spread, and assumed a spindle-like morphology after only 4 hours in culture (Fig. 3a,b). After 1 day in culture, MSCs exhibited thin and elongated protrusions and produced an interconnected network with adjacent cells. In contrast

to previous reports, cell adhesion and spread areas in 2D did not increase as a function of increasing hydrogel stiffness [56,57], indicating that hydrogel mechanical properties are not the driving force for the differences in cell response or that the magnitude changes are not great enough to observe an altered behavior. These results can be potentially explained by the fibrillar network that not only provides a provisional hierarchical ECM that confers mechanical support and ECM topography, but also contains numerous binding domains that mediates interactions with cells, ECM proteins and secreted growth factors [58–60].

3.2. Hyaluronic acid granular hydrogels containing embedded platelet lysate fibrillar proteins

3.2.1. Microgel synthesis and characterization

The assembling of building blocks into 3D scaffolds has emerged as a promising new approach to engineer hydrogels endowed with modular biochemical and biophysical cues [12]. We modified the previously optimized PL-NorHA approach to produce microgels, and thus increase the more widespread applications of the hydrogel.

A previously developed microfluidic device was modified to produce water-in-oil droplets of PL-NorHA or NorHA at 1 wt.% and 2 wt.% macromer concentrations (Fig. 4a) [17]. NorHA (containing clotting factors) and PL were introduced in the Y-shaped microfluidic chip through two separate channels at varying flow rate ratios, converging into a single channel with laminar flow. The physical separation of both solutions is crucial to avoid clogging in the microfluidic channels due to the enzymatic cleavage of fibrinogen that starts the self-assembly of fibrin. This process typically takes around 5-10 minutes, but its initial triggering is sufficient to promote the agglomeration of fibrin fibers throughout the tubing and device channels [39,43]. This single channel was then pinched-off by the immiscible continuous phase (i.e., oil with nonionic surfactant) to produce water-in-oil droplets. The introduction of a serpentine path then improves the mixing within the droplets through chaotic advection [61], while increasing the residence time on chip to allow fibrin polymerization. The droplets were transferred through tubing and crosslinked with visible light to form microgels, which were subsequently washed from oil and surfactant into buffer.

The incorporation of fluorescein-labeled dextran during microgel formation allowed the analysis of their morphology, including size and roundness (Fig. 4b,c). As previously demonstrated in PL-NorHA hydrogels, microgels containing PL produced a homogeneous and hierarchical fibrin network that was visualized by confocal reflectance (Fig. 4b-ii). Spherical microgels had an average diameter of 120 ± 12 μm (1 wt.% NorHA), 126 ± 17 μm (1 wt.% PL-NorHA), 100 ± 8 μm (2 wt.% NorHA) and 119 ± 21 μm (2 wt.% PL-NorHA), (Fig. 4c-i,ii). Previous studies reported that microgel dimensions are readily altered through the size of microchannels or precursor flow rates [12,62]. Although not tested here, alterations in the size and morphology of microgels could be used to meet the requirements of specific biomedical applications.

Microgel degradation was assessed for over one week through the release of uronic acid and total proteins, including in the presence of hyaluronidase (Fig. 4d). As shown with hydrogels, microgels exhibited degradation in the presence of hyaluronidase, which was faster with the lower NorHA concentration (Fig. 4d-i, iii). Moreover, the majority of PL-NorHA microgels degraded at a faster rate than NorHA formulations and generally microgels degraded more quickly than hydrogels of the same formulations (Fig. 2b). PL-NorHA microgels were further characterized for the release of total proteins (Fig. 4d-ii, iv). Microgels generally exhibited a lower initial release of proteins than PL-NorHA hydrogels (11 ± 3 %, 2 wt.% PL-NorHA microgels without hyaluronidase), which can be explained by the initial removal of the unbound proteins during the several washing steps from oil into buffer. Although we did not investigate the loading efficiency of PL-derived proteins in both systems, we believe that the microgel fabrication process (e.g., washing) could reduce protein loading.

After the first timepoint, a steady release of PL-derived proteins was observed from PL-NorHA microgels, corresponding to the inherent protein diffusion and degradation of the polymeric networks. At the end of 7 days, 41 ± 7 % and 69 ± 3 % of the total proteins were released from 2 wt.% PL-NorHA microgels in absence or with 0.005 mg. mL^{-1} of hyaluronidase, respectively. Thus, we observed that microgel stability and the rate of therapeutic-relevant protein delivery can be tailored by varying the crosslink density microgels, as well as the local hyaluronidase concentration. There are a number of parameters that can be modulated for more complex delivery profiles, such as the combination of microgels of varying stability and composition to recreate a microenvironment with modular properties over time [19].

3.2.2. Granular hydrogel rheological characterization

Microgels were jammed by vacuum filtration into granular hydrogels to allow physical interactions between the microgels so that they behave as solid extrudable materials, as previously demonstrated [12]. To better understand the potential injectability of these systems, the rheological behavior and structure of granular hydrogels were investigated (Fig. 5). Oscillatory shear rheometry results demonstrated that the increase in concentration of NorHA polymer from 1 to 2 wt.% within microgels increased the granular hydrogel storage modulus by up to one order of magnitude (Fig. 5a-i, iv). In agreement with observations in hydrogels, the presence of PL significantly decreased the granular hydrogel storage modulus (from 77 ± 3 Pa to 234 ± 2 Pa, 2 wt.% NorHA and PL-NorHA, respectively); however, solid-like properties (G' > G'') were observed in all tested conditions. Similar to our previous studies [17], granular hydrogels behaved rheologically as shear-thinning and self-healing materials, allowing their extrusion using minimal force without altering their initial properties. Both granular hydrogels from microgels of varied concentrations (1 wt.% and 2 wt.%) exhibited shear yielding with increased strains (Fig. 5a-ii, v). When subjected to high strains, jammed microgels demonstrated disruption of the contacts between particles as evident by the decreased storage moduli [17]. The self-recovery behavior was observed in all granular hydrogels through a series of high (500%) and low (0.5%) strains. After being subjected to high strains, the materials exhibited a rapid recovery of the solid-like behavior (Fig. 4a-iii, vi). Thus, the cyclic strain sweeps showed that granular hydrogels are able to recover their storage moduli upon reduction of applied strains, which demonstrates its rapid self-healing properties [63]. Based on their mechanical stability and mechanical recovery properties, granular hydrogels are suitable for several potential applications, including as inks for 3D printing or as injectable formulations for rapid localized delivery in a clinical or emergency setting.

To better understand the granular hydrogel structure, the microgels were incubated with rhodamine thiols for visualization before jamming. After vacuum filtration, 1 wt.% NorHA and PL-NorHA formulations exhibited very little porosity, as the microgels deformed during processing. The 2 wt.% PL-NorHA formulation exhibited increased porosity when compared to the 1 wt.% formulations, but was more dense than the 2 wt.% NorHA condition. These results can be potentially explained by the viscoelastic nature of microgel formulations, since the jamming of the microgels with low mechanics (1 wt.% PL-NorHA < 1 wt.% NorHA < 2 wt.% PL-NorHA < 2 wt.% NorHA) increased their packing density (1 wt.% PL-NorHA > 1 wt.% NorHA > 2 wt.% PL-NorHA > 2 wt.% NorHA) and subsequently decreased area between building blocks (Fig. 5b). The porosity of granular hydrogels can influence how the material

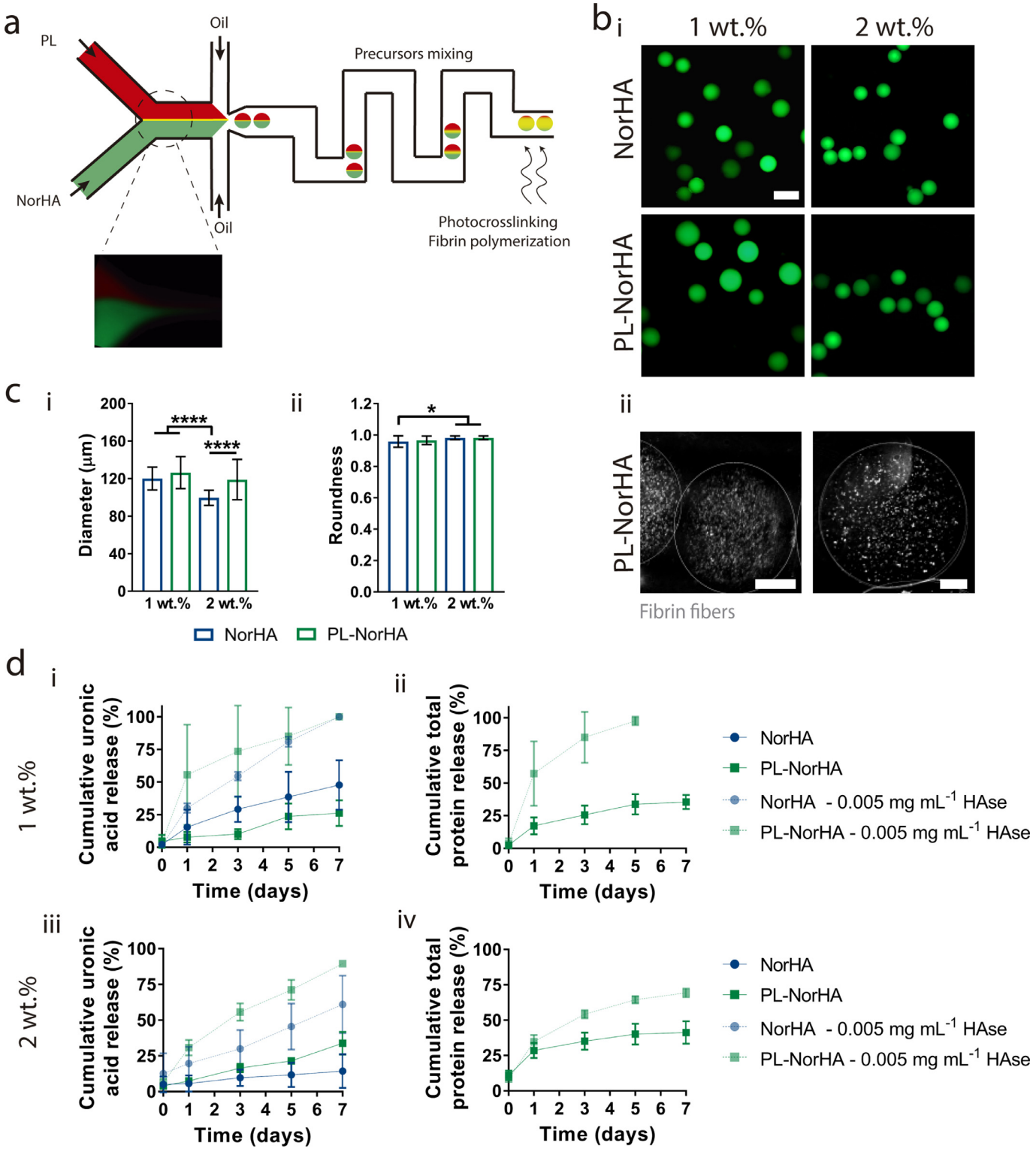

Fig. 4. Microgel fabrication and characterization. a) Schematic of the microfluidic device for the formation of water-in-oil droplets, where the PL (or PBS for NorHA alone microgels) (red) and NorHA (with clotting factors) (green) solutions are introduced and mixed down a serpentine path for fibrin polymerization and subsequently crosslinked with light exposure. b) Representative (i) fluorescent images of FITC-dextran (green) labeled 1 wt.% and 2 wt.% NorHA and PL-NorHA microgels and (ii) confocal reflectance images to detect fibrin fibers (gray) for 1 wt.% and 2 wt.% PL-NorHA microgels. c) Quantification of microgel (i) diameter distributions (n=34 microgels, mean ± SD, * $p < 0.05$, one-way ANOVA with Tukey's multiple comparisons test), and (ii) roundness, (n=34 microgels, mean ± SD, * $p < 0.05$, one-way ANOVA with Tukey's multiple comparisons test). d) Cumulative uronic acid and total protein release during the degradation of (i, ii) 1 wt.% and (iii, iv) 2 wt.% microgels when incubated in PBS alone or with hyaluronidase (HAse) at 0.005 mg mL^{-1}. Scale bars: 200 μm (b-i), 50 μm (b-ii and iii).

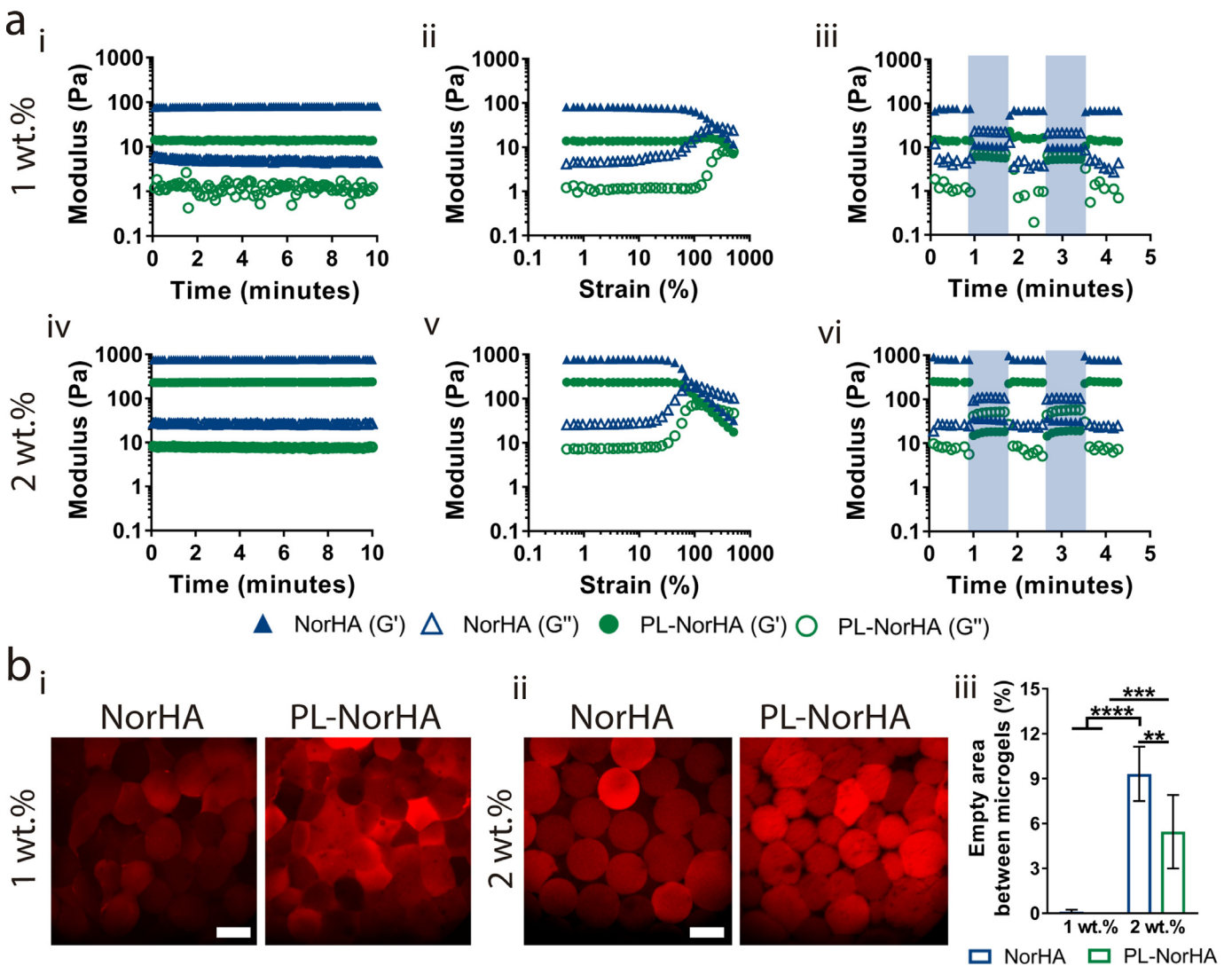

Fig. 5. Rheological and morphological characterization of jammed NorHA and PL-NorHA granular hydrogels. a) Oscillatory shear rheometry including time sweeps (1 Hz and 0.5% strain), strain sweeps (0.5% to 500% strain and 1 Hz) and cycles through low (0.5% strain, 1 Hz, unshaded) and high (500% strain, 1 Hz, shaded) strains for granular hydrogels from (i-iii) 1 wt.% and (iv-vi) 2 wt.% microgels. b) Representative fluorescence images of rhodamine-labelled (red) granular hydrogels from (i) 1 wt.% and (ii) 2 wt.% NorHA and PL-NorHA microgels, and (iii) quantification of the empty area between microgels (n=5 images , mean ± SD, ** $p < 0.01$, *** $p < 0.001$, **** $p < 0.0001$ one-way ANOVA with Tukey's multiple comparisons test). (note: PL-NorHA jammed microgels from 1 wt. % showed an empty area between microgels of 0%). Scale bars: 100 μm (b).

behaves under load, as well as cell interactions since an adequate pore space between microgels is needed for the transport of oxygen, metabolites and nutrients [64].

3.2.3. 3D printed granular hydrogels and in vitro cell response

Microgels were jammed into granular hydrogels and used as injectable inks for 3D printing. To assess the printability of the microgels inks, single filaments that contained microgels with FITC-dextran were printed onto a glass surface and visualized by fluorescence microscopy (Fig. 6a). Due to their granular structure, the microgel inks were easily extruded to form a uniform filament that displayed a densely packed microgel morphology. Jammed microgels inks were further 3D printed to fabricate 3D constructs (Fig. 6b-i), as previously optimized [17]. The softer jammed microgels resulted in stable 3D constructs for up to seven days in buffer (Fig. 6b-ii, iii, v); however, jammed microgels inks from more highly crosslinked NorHA particles (2 wt.%) resulted in structures that were easily disrupted (Fig. 6b-iv.). Besides their structural integrity, the printed constructs also showed a high shape fidelity (Fig. 6b-ii, iii and v) to the printed cuboid structure (Fig. 6b-i).

The jamming process is adequate to obtain stable granular hydrogels in which the microporous structure is maintained without needing further processing, as long as the microgels are soft enough to deform when packed together (Fig. 6b). Several groups have also proposed a variety of chemistries to anneal microgels to maintain their initial structure, namely enzymatic, light induced radical polymerization, and/or carbodiimide chemistry [12,64].

As an initial proof of concept of using these granular cells to support cell culture, 1 wt.% NorHA and PL-NorHA microporous scaffold constructs were cultured with MSCs under serum-free conditions and visualized after 1 and 7 days of *in vitro* culture (Fig. 6c). Cells were seeded throughout granular hydrogels by mixing the cells with microgels before jamming.

At the beginning of the culture, cells were uniformly distributed throughout the granular hydrogels. MSCs seeded on NorHA microgels exhibited rounded morphologies (Fig. 6c-i), similar to that observed in NorHA hydrogels (Fig. 3a). On the other hand, after only 1 day in culture, the interconnected microporous space in

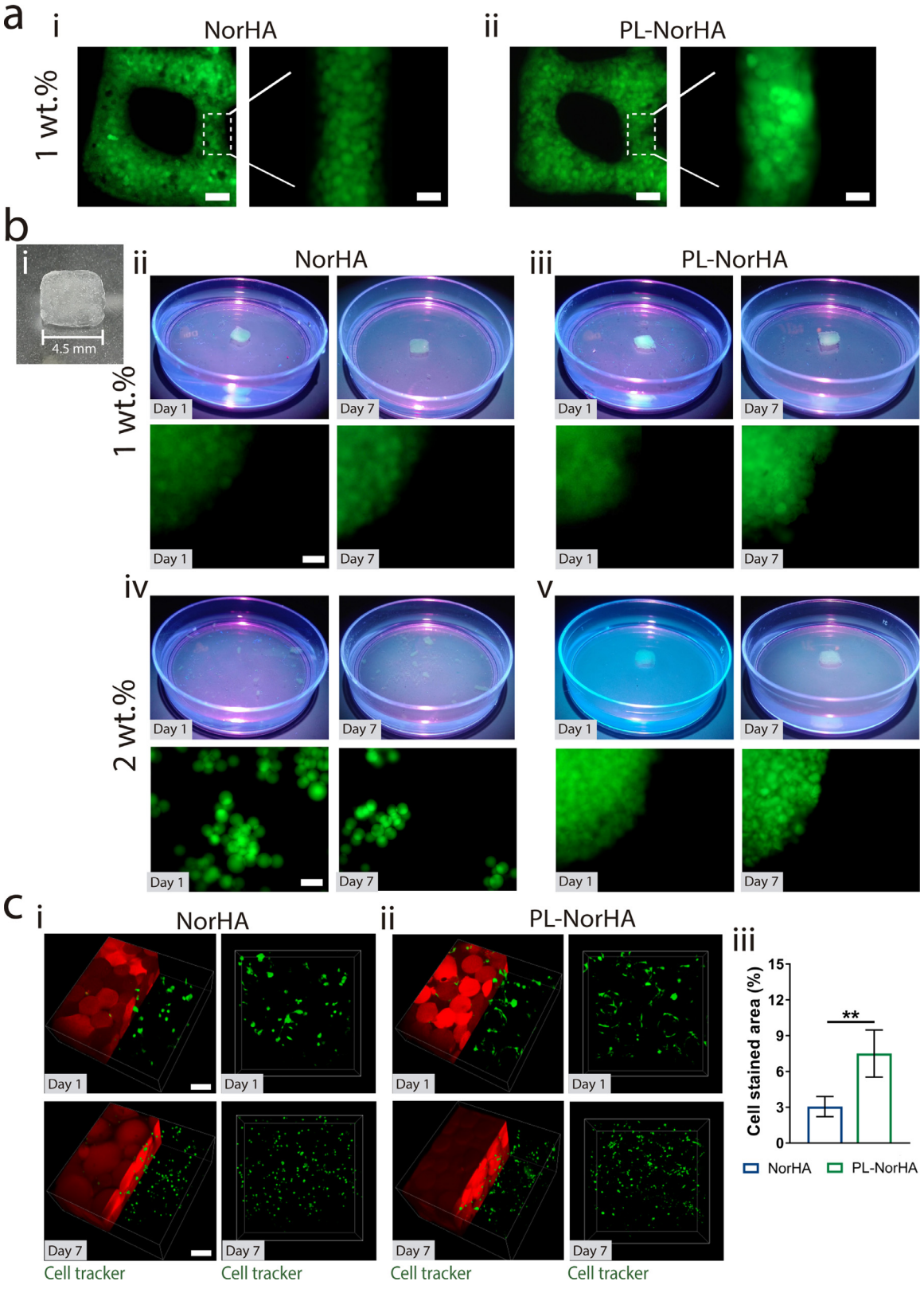

Fig. 6. 3D printed structure stability and interactions with MSCs. a) Fluorescent images of lattice structures from 3D printed granular hydrogels from 1 wt.% microgels containing FITC-dextran (green) from (i) NorHA or (ii) PL-NorHA. b) Macroscopic image of (i) cuboid structure with 1 wt.% NorHA jammed microgels ink. Macroscopic and fluorescent images of cuboid structure after 1 or 7 days of incubation in buffer, when fabricated from granular from (ii-iii) 1 wt.% and (iv-v) 2 wt.% NorHA or PL-NorHA microgels. c) Representative fluorescence images of MSCs (Cell Tracker™ fluorescent probes: green) after 1 or 7 days of serum-free culture in granular hydrogels from 1 wt.% microgels containing rhodamine (red) from (i) NorHA or (ii) PL-NorHA; (iii) quantification of the cell tracker stained area (Cell Tracker™ fluorescent probes: green) at day 1 (n=5 images, mean ± SD, ** $p < 0.01$, student t-test with two-tailed criteria). (note: granular hydrogels from 2 wt. % microgels were not stable with culture for NorHA, so this was not performed). Scale bars: 500 μm (a-i and ii), 200 μm (b), 100 μm (a-i inset and ii inset, c-i and ii).

PL-NorHA microgels promoted substantial cell spreading and the formation of 3D cellular networks (Fig. 6c-i-iii). Besides the crucial role of PL-derived proteins on promoting efficient cell adhesion and survival, it is also important to highlight the importance of the hierarchical fibrin network that provides numerous cell-anchorage sites. These results demonstrated that the proposed bioinstructive platform provides an ECM mimetic porous network and human-derived biomolecules reservoir that could modulate a number of complex cellular responses at the single cell level.

4. Conclusions

In this study, we developed and unique approach to incorporate therapeutically-relevant molecules that mimic the hierarchical fibrillar architecture and composition of the native ECM into hydrogels and microgels. Specifically, this was achieved through the incorporation of PL into covalently crosslinked HA hydrogels, where the physical properties and protein delivery stemming from PL were modulated by varying the HA concentration. These bioactive cues contributed to greater MSC spreading when compared to hydrogel formulations without PL. Jammed microgels of these formulations displayed shear-thinning and self-healing properties, enabling administration through minimally invasive approaches as well as processing into structures with 3D printing. Finally, the incorporation of PL into printed constructs enabled the *in vitro* culture of MSCs under serum-free conditions.

Statement of significance

Recreating the biochemical and biophysical cues of the hierarchical extracellular matrix (ECM) with engineered biomaterials remains challenging. Inspired by natural wound healing mechanisms, here we develop hyaluronic acid microgels containing platelet lysate (PL), a human source of biologically-active and structural proteins. These microgels are assembled as elementary units to produce injectable granular hydrogels featuring embedded fibrillar networks, to resemble the hierarchical architecture of ECM. The addition of PL to the microgels enhances cell adhesion proliferation. In addition, jammed microgels show shear-thinning behavior that facilitates injectability, and the addition of PL enhances inter-particle interactions and microgel cohesion post-injection. Together, this strategy offers a promising approach to improve the bioactivity of hyaluronic acid-hydrogels to meet the complex demands of functional tissue repair.

Declaration of Competing Interest

The authors declare that they have no known competing financial interests or personal relationships that could have appeared to influence the work reported in this paper.

Acknowledgement

The authors acknowledge the financial support from FCT/MCTES (Fundação para a Ciência e a Tecnologia/ Ministério da Ciência, Tecnologia, e Ensino Superior), the Fundo Social Europeu através do Programa Operacional do Capital Humano (FSE/POCH) in the framework of PhD grant PD/59/2013 – PD/BD/113807/2015 (BBM) and the National Science Foundation MRSEC (DMR-1720530). The authors would like to thank M. Chen, M. Davidson, J. Galagarra, T. Qazi, S. Uman, A. Brito and C. Loebel for helpful discussions.

Supplementary materials

Supplementary material associated with this article can be found, in the online version, at doi:10.1016/j.actbio.2020.10.040.

References

[1] R. Perez-Castillejos, Replication of the 3D architecture of tissues, Mater. Today 13 (2010) 32–41.
[2] J.K. Mouw, G. Ou, V.M. Weaver, Extracellular matrix assembly: a multiscale deconstruction, Nat. Rev. Mol. Cell Biol. 15 (2014) 771–785.
[3] R.O. Hynes, A. Naba, Overview of the matrisome–an inventory of extracellular matrix constituents and functions, Cold Spring Harb. Perspect. Biol. 4 (2012) a004903.
[4] K.H. Vining, D.J. Mooney, Mechanical forces direct stem cell behaviour in development and regeneration, Nat. Rev. Mol. Cell BiOL. 18 (2017) 728–742.
[5] L. Macri, D. Silverstein, R.A.F. Clark, Growth factor binding to the pericellular matrix and its importance in tissue engineering, Adv. Drug Deliv. Rev. 59 (2007) 1366–1381.
[6] N.S. Gandhi, R.L. Mancera, The Structure of Glycosaminoglycans and their Interactions with Proteins, Chem. Biol. Drug Des. 72 (2008) 455–482.
[7] V. Vogel, Unraveling the Mechanobiology of Extracellular Matrix, Annu. Rev. Physiol. 80 (2018) 353–387.
[8] R.O. Hynes, The Extracellular Matrix: Not Just Pretty Fibrils, Science 326 (2009) 1216–1219.
[9] A.S. Hoffman, Hydrogels for biomedical applications, Adv. Drug Deliv. Rev. 54 (2002) 3–12.
[10] X. Tong, F. Yang, Recent Progress in Developing Injectable Matrices for Enhancing Cell Delivery and Tissue Regeneration, Adv. Healthc. Mater. 7 (2018) e1701065.
[11] R. Dimatteo, N.J. Darling, T. Segura, In situ forming injectable hydrogels for drug delivery and wound repair, Adv. Drug Deliv. Rev. 127 (2018) 167–184.
[12] A.C. Daly, L. Riley, T. Segura, J.A. Burdick, Hydrogel microparticles for biomedical applications, Nat. Rev. Mater. 5 (2020) 20–43.
[13] M.D. Neto, M.B. Oliveira, J.F. Mano, Microparticles in Contact with Cells: From Carriers to Multifunctional Tissue Modulators, Trends Biotechnol 37 (() (2019) 1011–1028.
[14] S. Xin, J. Dai, C.A. Gregory, A. Han, D.L. Alge, Creating Physicochemical Gradients in Modular Microporous Annealed Particle Hydrogels via a Microfluidic Method, Adv. Funct. Mater. 30 (2020) 1907102.
[15] D.R. Griffin, W.M. Weaver, P.O. Scumpia, D. Di Carlo, T. Segura, Accelerated wound healing by injectable microporous gel scaffolds assembled from annealed building blocks, Nat. Mater. 14 (2015) 737–744.
[16] S. Xin, D. Chimene, J.E. Garza, A.K. Gaharwar, D.L. Alge, Clickable PEG hydrogel microspheres as building blocks for 3D bioprinting, Biomater. Sci. 7 (2019) 1179–1187.
[17] C.B. Highley, K.H. Song, A.C. Daly, J.A. Burdick, Jammed Microgel Inks for 3D Printing Applications, Adv. Sci. 6 (2019) 1801076.
[18] J. Koh, D.R. Griffin, M.M. Archang, A.-C. Feng, T. Horn, M. Margolis, D. Zalazar, T. Segura, P.O. Scumpia, D. Di Carlo, Enhanced In Vivo Delivery of Stem Cells using Microporous Annealed Particle Scaffolds, Small 15 (2019) 1903147.
[19] M.D. Neto, M.B. Oliveira, J.F. Mano, Microparticles in Contact with Cells: From Carriers to Multifunctional Tissue Modulators, Trends Biotechnol (2019) 1011–1028.
[20] C. Wang, Y. Gong, Y. Zhong, Y. Yao, K. Su, D.-A. Wang, The control of anchorage-dependent cell behavior within a hydrogel/microcarrier system in an osteogenic model, Biomaterials 30 (2009) 2259–2269.
[21] B.P. Toole, Hyaluronan: from extracellular glue to pericellular cue, Nat. Rev. Cancer 4 (2004) 528–539.
[22] J.A. Burdick, G.D. Prestwich, Hyaluronic Acid Hydrogels for Biomedical Applications, Adv. Mater. 23 (2011) H41–H56.
[23] C.B. Highley, G.D. Prestwich, J.A. Burdick, Recent advances in hyaluronic acid hydrogels for biomedical applications, Curr. Opin. Biotech. 40 (2016) 35–40.
[24] K.J. Wolf, S. Kumar, Hyaluronic Acid, Incorporating the Bio into the Material, ACS Biomater. Sci. Eng. (2019) 3753–3765.
[25] Y. Zhang, P. Heher, J. Hilborn, H. Redl, D.A. Ossipov, Hyaluronic acid-fibrin interpenetrating double network hydrogel prepared in situ by orthogonal disulfide cross-linking reaction for biomedical applications, Acta Biomater 38 (2016) 23–32.
[26] Y.D. Park, N. Tirelli, J.A. Hubbell, Photopolymerized hyaluronic acid-based hydrogels and interpenetrating networks, Biomaterials 24 (2003) 893–900.
[27] B.B. Mendes, M. Gómez-Florit, P.S. Babo, R.M. Domingues, R.L. Reis, M.E. Gomes, Blood derivatives awaken in regenerative medicine strategies to modulate wound healing, Adv. Drug Deliv. Rev. 129 (2018) 376–393.
[28] W.M. Gramlich, I.L. Kim, J.A. Burdick, Synthesis and orthogonal photopatterning of hyaluronic acid hydrogels with thiol-norbornene chemistry, Biomaterials 34 (2013) 9803–9811.
[29] S.T. Robinson, A.M. Douglas, T. Chadid, K. Kuo, A. Rajabalan, H. Li, I.B. Copland, T.H. Barker, J. Galipeau, L.P. Brewster, A novel platelet lysate hydrogel for endothelial cell and mesenchymal stem cell-directed neovascularization, Acta Biomater 36 (2016) 86–98.
[30] C. Loebel, R.L. Mauck, J.A. Burdick, Local nascent protein deposition and remodelling guide mesenchymal stromal cell mechanosensing and fate in three--dimensional hydrogels, Nat. Mater. 18 (2019) 883–891.
[31] J.E. Mealy, J.J. Chung, H.-H. Jeong, D. Issadore, D. Lee, P. Atluri, J.A. Burdick, Injectable Granular Hydrogels with Multifunctional Properties for Biomedical Applications, Adv. Mater. 30 (2018) 1705912.
[32] C.B. Highley, C.B. Rodell, J.A. Burdick, Direct 3D Printing of Shear-Thinning Hydrogels into Self-Healing Hydrogels, Adv. Mater. 27 (2015) 5075–5079.

[33] C.A. Ramsden, A. Bankier, T.J. Brown, P.S.J. Cowen, G.I. Frost, D.D. McCallum, V.P. Studdert, J.R.E. Fraser, A new disorder of hyaluronan metabolism associated with generalized folding and thickening of the skin, Pediatrics 136 (2000) 62–68.
[34] E.L. Hiltunen, M. Anttila, A. Kultti, K. Ropponen, J. Penttinen, M. Yliskoski, A.T. Kuronen, M. Juhola, R. Tammi, M. Tammi, Elevated hyaluronan concentration without hyaluronidase activation in malignant epithelial ovarian tumors, Cancer Res 62 (2002) 6410–6413.
[35] M.H. Chen, J.J. Chung, J.E. Mealy, S. Zaman, E.C. Li, M.F. Arisi, P. Atluri, J.A. Burdick, Injectable Supramolecular Hydrogel/Microgel Composites for Therapeutic Delivery, Macromol. Biosci. 19 (2019) 1800248.
[36] T. Bitter, H.M. Muir, A modified uronic acid carbazole reaction, Anal. Biochem. 4 (1962) 330–334.
[37] H. Shih, C.-C. Lin, Cross-Linking and Degradation of Step-Growth Hydrogels Formed by Thiol–Ene Photoclick Chemistry, Biomacromolecules 13 (2012) 2003–2012.
[38] B.D. Fairbanks, M.P. Schwartz, A.E. Halevi, C.R. Nuttelman, C.N. Bowman, K.S. Anseth, A Versatile Synthetic Extracellular Matrix Mimic via Thiol-Norbornene Photopolymerization, Adv. Mater. 21 (2009) 5005–5010.
[39] E.A. Ryan, L.F. Mockros, J.W. Weisel, L. Lorand, Structural origins of fibrin clot rheology, Biophys. J. 77 (1999) 2813–2826.
[40] K.T. Dicker, L.A. Gurski, S. Pradhan-Bhatt, R.L. Witt, M.C. Farach-Carson, X. Jia, Hyaluronan: A simple polysaccharide with diverse biological functions, Acta Biomater 10 (2014) 1558–1570.
[41] J.C. Houck, R.H. Pearce, The mechanism of hyaluronidase action, Biochim. Biophys. Acta 25 (1957) 555–562.
[42] J.A. Burdick, C. Chung, X. Jia, M.A. Randolph, R. Langer, Controlled Degradation and Mechanical Behavior of Photopolymerized Hyaluronic Acid Networks, Biomacromolecules 6 (2005) 386–391.
[43] B.B. Mendes, M. Gómez-Florit, R.A. Pires, R.M.A. Domingues, R.L. Reis, M.E. Gomes, Human-based fibrillar nanocomposite hydrogels as bioinstructive matrices to tune stem cell behavior, Nanoscale 10 (2018) 17388–17401.
[44] M.M. Martino, P.S. Briquez, A. Ranga, M.P. Lutolf, J.A. Hubbell, Heparin-binding domain of fibrin(ogen) binds growth factors and promotes tissue repair when incorporated within a synthetic matrix, Proc. Natl. Acad. Sci. U.S.A. 110 (2013) 4563–4568.
[45] S. Kandoi, P.k.L, B. Patra, P. Vidyasekar, D. Sivanesan, V.S, R.K, R.S. Verma, Evaluation of platelet lysate as a substitute for FBS in explant and enzymatic isolation methods of human umbilical cord MSCs, Sci. Rep. 8 (2018) 12439.
[46] V. Pavlovic, M. Ciric, V. Jovanovic, P. Stojanovic, Platelet Rich Plasma: a short overview of certain bioactive components, Open Med 11 (2016) 242–247.
[47] S.G. Boswell, B.J. Cole, E.A. Sundman, V. Karas, L.A. Fortier, Platelet-Rich Plasma: A Milieu of Bioactive Factors, Arthroscopy 28 (2012) 429–439.
[48] H. Hemeda, B. Giebel, W. Wagner, Evaluation of human platelet lysate versus fetal bovine serum for culture of mesenchymal stromal cells, Cytotherapy 16 (2014) 170–180.
[49] C.R. Silva, P.S. Babo, M. Gulino, L. Costa, J.M. Oliveira, J. Silva-Correia, R.M.A. Domingues, R.L. Reis, M.E. Gomes, Injectable and tunable hyaluronic acid hydrogels releasing chemotactic and angiogenic growth factors for endodontic regeneration, Acta Biomater 77 (2018) 155–171.
[50] M.C. Phipps, Y. Xu, S.L. Bellis, Delivery of platelet-derived growth factor as a chemotactic factor for mesenchymal stem cells by bone-mimetic electrospun scaffolds, PLoS One 7 (2012) e40831.
[51] M. Matsui, Y. Tabata, Enhanced angiogenesis by multiple release of platelet-rich plasma contents and basic fibroblast growth factor from gelatin hydrogels, Acta Biomater 8 (2012) 1792–1801.
[52] E. Jooybar, M.J. Abdekhodaie, M. Alvi, A. Mousavi, M. Karperien, P.J. Dijkstra, An injectable platelet lysate-hyaluronic acid hydrogel supports cellular activities and induces chondrogenesis of encapsulated mesenchymal stem cells, Acta Biomater 83 (2019) 233–244.
[53] F. Re, L. Sartore, V. Moulisova, M. Cantini, C. Almici, A. Bianchetti, C. Chinello, K. Dey, S. Agnelli, C. Manferdini, S. Bernardi, N.F. Lopomo, E. Sardini, E. Borsani, L.F. Rodella, F. Savoldi, C. Paganelli, P. Guizzi, G. Lisignoli, F. Magni, M. Salmeron-Sanchez, D. Russo, 3D gelatin-chitosan hybrid hydrogels combined with human platelet lysate highly support human mesenchymal stem cell proliferation and osteogenic differentiation, J. Tissue Eng 10 (2019) 2041731419845852.
[54] A.B. Moshnikova, V.N. Afanasyev, O.V. Proussakova, S. Chernyshov, V. Gogvadze, I.P. Beletsky, Cytotoxic activity of 1-ethyl-3-(3-dimethylaminopropyl)-carbodiimide is underlain by DNA interchain cross-linking, Cell. Mol. Life Sci. 63 (2006) 229–234.
[55] P.R. Umashankar, P.V. Mohanan, T.V. Kumari, Glutaraldehyde treatment elicits toxic response compared to decellularization in bovine pericardium, Toxicol. Int. 19 (2012) 51–58.
[56] D.E. Discher, D.J. Mooney, P.W. Zandstra, Growth Factors, Matrices, and Forces Combine and Control Stem Cells, Science 324 (2009) 1673–1677.
[57] T. Yeung, P.C. Georges, L.A. Flanagan, B. Marg, M. Ortiz, M. Funaki, N. Zahir, W. Ming, V. Weaver, P.A. Janmey, Effects of substrate stiffness on cell morphology, cytoskeletal structure, and adhesion, Cell Motil. Cytoskeleton 60 (2005) 24–34.
[58] N. Laurens, P. Koolwijk, M.P.M. De Maat, Fibrin structure and wound healing, J. Thromb. Haemost. 4 (2006) 932–939.
[59] A.C. Brown, T.H. Barker, Fibrin-based biomaterials: Modulation of macroscopic properties through rational design at the molecular level, Acta Biomater 10 (2014) 1502–1514.
[60] V.K. Lishko, N.P. Podolnikova, V.P. Yakubenko, S. Yakovlev, L. Medved, S.P. Yadav, T.P. Ugarova, Multiple Binding Sites in Fibrinogen for Integrin $\alpha M\beta 2$ (Mac-1), J, Biol. Chem. 279 (43) (2004) 44897–44906.
[61] H. Song, J.D. Tice, R.F. Ismagilov, A Microfluidic System for Controlling Reaction Networks in Time, Angew. Chem. Int. Ed. 42 (2003) 768–772.
[62] L.P.B. Guerzoni, J.C. Rose, D.B. Gehlen, A. Jans, T. Haraszti, M. Wessling, A.J.C. Kuehne, L. De Laporte, Cell Encapsulation in Soft, Anisometric Poly(ethylene) Glycol Microgels Using a Novel Radical-Free Microfluidic System, Small 15 (2019) 1900692.
[63] C. Loebel, C.B. Rodell, M.H. Chen, J.A. Burdick, Shear-thinning and self-healing hydrogels as injectable therapeutics and for 3D-printing, Nat. Protoc. 12 (2017) 1521–1541.
[64] E. Sideris, D.R. Griffin, Y. Ding, S. Li, W.M. Weaver, D. Di Carlo, T. Hsiai, T. Segura, Particle Hydrogels Based on Hyaluronic Acid Building Blocks, ACS Biomater. Sci. Eng. 2 (2016) 2034–2041.